

Boundary Layer Measurements on a Slender Body using Long-Distance PIV

P. Manovski¹, M. Jones¹, S. Henbest¹, Y. Xue^{1,2} and M. Giacobello¹

¹Aerospace Division, Defence Science and Technology Group, Victoria 3207, Australia

²Australian Maritime College, University of Tasmania, Tasmania 7248, Australia

Abstract

This study reports the development and application of long-distance high magnification Particle Image Velocimetry (PIV) to measure the mean and fluctuating velocity components in a turbulent boundary layer. A 400 mm lens coupled with an extension tube and a novel aperture control mechanism has enabled high resolution images at a working distance of 1.5 m. The PIV results were found to compare well with established probe measurements along a slender axisymmetric body. The boundary layer thickness and mean streamwise velocity was found to conform to a traditional turbulent boundary layer in the parallel mid-body section of the body.

Introduction

Advances in computational fluid dynamic (CFD) models, coupled with increases in the available computing infrastructure has allowed scale-resolving simulations to be run at higher Reynolds numbers (approaching full-scale). This has driven a requirement to perform validating experiments in large-scale facilities. The drawback of using non-intrusive optical methods such as Particle Image Velocimetry (PIV) in large-scale facilities compared with smaller scale research facilities is the reduced resolution of measurements arising from the longer working distances thus limiting image magnification. For this study an effort to overcome this limitation was made by employing a large focal length lens to conduct a long-distance high magnification PIV to obtain near wall measurements over a slender axisymmetric body that is representative of a bare hull submarine. From these measurements boundary layer profiles and inferred wall skin friction estimates were obtained. Others have used similar methods on turbulent boundary layers (see [3] and cited references), although generally at smaller working distances (<1 m) compared with the 1.5 m working distance in the current study.

For this study the performance of PIV in measuring near wall flow fields was validated by comparing the results against traditional techniques. This validation will provide confidence in using high-magnification PIV in regions around a fully appended submarine model that are inaccessible with probes, such as directly upstream of appendages and in regions of reverse flow or high flow angularity where probe measurements are generally invalid.

Test Facility and Model

The experiments were conducted at the Defence Science & Technology (DST) Group Low Speed Wind Tunnel with test section dimensions of $2.74 \times 2.13 \text{ m}^2$ (width \times height) and a reported free stream turbulence intensity of 0.4% [4]. The test model was a slender axisymmetric body (DST Generic Submarine bare hull form) with a 273.66 mm diameter (D) and a length (L) of 2000 mm. Lee and Jones [7] provide further detail of the model geometry used in this test. The model was mounted on twin aerofoil sectioned supports from the bottom, as shown in figure 1. In order to transition the flow to a fully turbulent state, Cadcut trip dots of 0.29 mm in height were located circumferen-

tially 99 mm (0.05L) downstream from the nose. Measurements by Henbest and Jones [5] showed that the boundary layer flow was fully turbulent. During all tests the model was aligned with zero incidence and the nominal freestream velocity was $U_\infty = 28.8 \text{ m/s}$, corresponding to a Reynolds number based on model length of approximately 4×10^6 .

Experimental Methodology

Long-distance high magnification PIV measurements were obtained at different axial locations along the model. The PIV boundary layers measurements were then compared with classical boundary layer measurement techniques, such as pitot probe and hotwire anemometer. The skin friction was also determined with a Preston tube.

Particle Image Velocimetry

To perform PIV, the wind tunnel flow was seeded with $\approx 1 \mu\text{m}$ diameter aerosol particles of di-ethyl-hexyl-sebacat (DEHS). A New Wave Solo 200XT Nd:YAG dual-pulse laser with 160 mJ per pulse was positioned above the test section. A series of light sheet optics produced a 1.5 mm thick laser sheet at the model surface and was aligned with the streamwise direction. The PIV setup is shown in figure 1.

A Nikon AF-S 400 mm G f2.8 lens was used to provide PIV measurements of the near wall region with a magnification factor of 0.33. The minimum focus distance of the lens is 2.9 m, thus to achieve the desired working distance of 1.5 m a 88 mm adjustable extension tube was manufactured and fitted to the lens (see figure 2). Typically, the lens aperture setting (or f-stop) is adjusted during the setup of PIV experiments as it is related to important parameters such as the particle intensity counts, the imaged particle diameter and the depth-of-field. Since the current generation of Nikon G-style lenses do not have a manual aperture ring, a novel software operated actuator was employed to control the aperture setting. A Thorlabs stepper motor actuator (ZFS06) with 6 mm of travel along with a motor controller (KST101) was used to adjust the lens aperture iris by means of

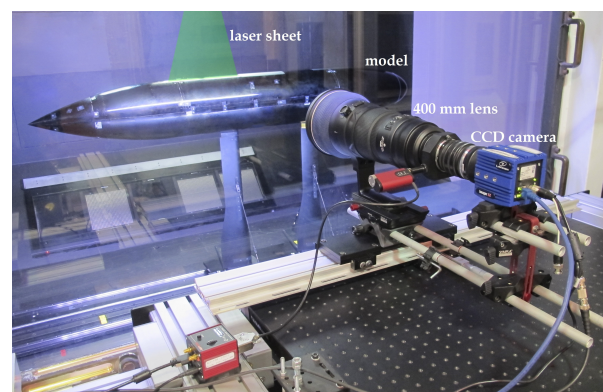


Figure 1: The PIV setup and axisymmetric model mounted with twin aerofoil sectioned supports.

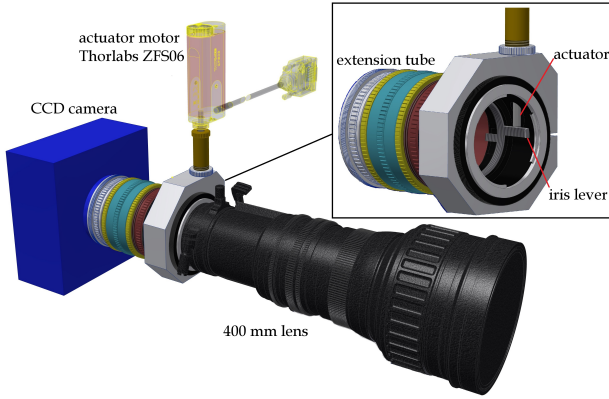


Figure 2: Optical setup including 400 mm lens with actuator motor and extension tube mounted to 29 MP camera. A close-up view of the lens aperture control mechanism showing actuator and lever that adjusts lens iris (inset).

a lever located on the lens as shown in figure 2 (inset). A calibration was performed by imaging a white background with a constant illumination light source. For a range of actuator settings the average image intensity of a number of images was calculated and a best-fit to the data was obtained using a logarithmic least squares regression. The corresponding f-stop values were then determined by using an approximation that each f-stop corresponds to half the incoming light (or image intensity) of the previous f-stop. Using this calibration curve the desired aperture can be set via software with all apertures (iris positions) available as well as finer increments. The software records the current set aperture position and enables return to previous positions. This feature ensures accurate repeatability during an experimental test campaign. The lens coupled with a 29 megapixel camera (LaVision Imager 29M) with $5.5 \mu\text{m}$ pixel pitch resulted in a spatial resolution of 59.4 px/mm . The imaged particle diameter was between 3-5 px. The pulse delay time was $8 \mu\text{s}$, resulting in a freestream displacement of about 16 px. In order to ensure converged statistical quantities a large batch of 6000 double-frame images were recorded at each axial station. The imaged field-of-view was approximately $110 \times 74 \text{ mm}^2$ in the streamwise and wall-normal directions, respectively. However, the 400 mm lens does suffer from optical distortions or pin-cushioning which resulted in out-of-focus particles around the perimeter of the image. In order to reduce the level of distortion the lens was operated at f-stop = 8 and the region of interest (i.e. the boundary layer) was centred in the image. The outer region of each image was then cropped and the final processed field-of-view was approximately $75 \times 55 \text{ mm}^2$.

DaVis 8.4 was used to process the PIV data with an initial interrogation window (IW) size of $64 \times 64 \text{ px}^2$ and a final IW size of $24 \times 24 \text{ px}^2$ with 75% overlap. The resulting vector resolution was 0.10 mm. An elliptical Gaussian weighting function is employed with 4:1 aspect ratio with the larger dimension in the flow direction. The use of more pixels in the direction perpendicular to the wall was avoided as it would smear the correlation peak due to the high wall normal gradients and contributions of different velocities. Hence the elliptical weighting function should result in improved accuracy in the vector field as the resulting displacement weights the local information higher than the pixel information further away and thus represents the local displacement better. Vector validation was performed using a neighbourhood (5×5 vectors) median filter with 2 px tolerance. The spurious vectors during a single instantaneous snapshot were on average less than 1% of the total vectors.

Hotwire Anemometer

A Dantec 55P05 boundary-layer normal hotwire was connected to a NASA designed constant-temperature hotwire anemometer [9]. The wire was operated at an over-heat ratio of 1.8 and using a square wave voltage injection the quadratic response was adjusted to be optimally damped with a response of at least 8 kHz. The anemometer top of bridge voltage was amplified and bucked to maximise data acquisition resolution and low pass filtered at 12.5 kHz. A Microstar DAP4000a/212 data acquisition processor with 14-bit A/D resolution for an input analogue voltage range of $\pm 10 \text{ V}$ was used to sample simultaneously the voltage outputs. The anemometer voltages were sampled at 20 kHz for a period of 20 s. A simple static calibration was performed resulting in a cubic curve fit between streamwise velocity and anemometer output voltage. The temperature during the hotwire tests was approximately 21.5°C and remained within 0.1°C during the acquisition time.

Pitot Tube

Mean flow boundary layer profiles were measured using a United Sensor boundary layer probe BA-025-12-C-11-650 with tube diameter, $d = 0.635 \text{ mm}$. The probe tip is flattened to half the tube diameter giving a tip thickness of 0.3175 mm and an effective wall distance of 0.159 mm . The probe pressure was referenced to the local static pressure tapping on the model to infer the local dynamic pressure on the total head tube. The pressures were monitored on two Baratron MKS 120 differential pressure transducers and the analogue output signals were sampled on the Microstar system (above) at a 200 Hz for a sample time of 10 s. The boundary layer probe (and hotwire) was attached to an overhead traverse mounted above the tunnel working section. The relative motion accuracy of the traverse was 0.01 mm.

Preston Tube

A Preston tube with a 0.60 mm outer diameter was used to obtain the wall skin friction along the model length. The relative pressure difference between the Preston tube and the local wall static pressure, ΔP , was measured using a Baratron MKS 120 transducer (above). The wall friction velocity, U_τ , and surface shear stress, τ_0 , were estimated from ΔP using the method of Patel [8] and as outlined in [6]. The skin friction coefficient, C_f , is given by

$$\frac{C_f}{2} = \frac{1}{2} \left(\frac{\tau_0}{\frac{1}{2} \rho U_\infty^2} \right) = \frac{U_\tau^2}{U_\infty^2}, \quad (1)$$

where U_∞ is the free stream velocity and ρ is the density of air.

Results

The PIV measurements were centred along the axial locations, $x/L = 0.25, 0.449, 0.65, 0.8$ and 0.9 . The ensemble averaged PIV flow fields are presented in figure 3 and show the boundary layer development along the model. Typical boundary layer flow can be seen in figure 4, an instantaneous PIV snapshot of the streamwise velocity (U) at $x/L = 0.65$.

Mean Flow Boundary Layer Profiles

Mean streamwise velocity (\bar{U}) profiles measured with PIV and pitot tube are compared against the logarithmic universal law of the wall function,

$$\frac{\bar{U}}{U_\tau} = \frac{1}{\kappa} \ln(z^+) + A, \quad (2)$$

where $z^+ = zU_\tau/\nu$ is the non-dimensional wall unit, A is the universal smooth wall constant and κ is the Karman constant. The traditional flat plate values of $A=5$ and $\kappa=0.41$ were used.

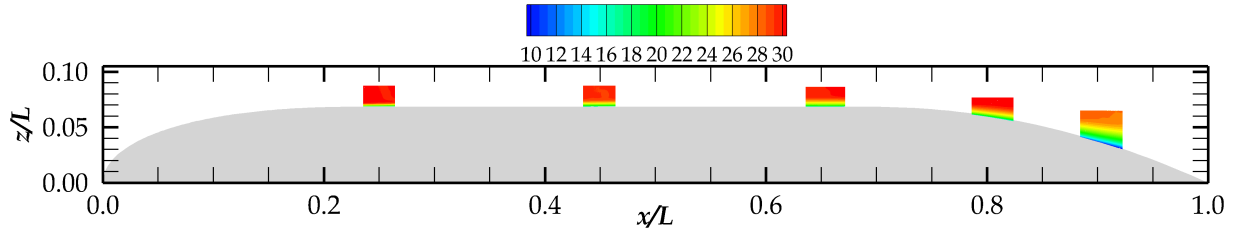


Figure 3: PIV near wall measurements at different locations along the slender body, colour coded by the mean streamwise velocity (\bar{U}).

For the PIV data the wall position was obtained directly from the images and was indicated by the laser surface reflection. Whereas aerodynamic loads upon the model and pitot probe led to relative movement between them, and as a consequence the initial wall position was inferred to be when the pressure readings just started to increase as the probe moved away from the surface and the value was a minimum. For both the PIV and pitot results the wall friction velocity was then obtained from a minimum least square fit to the logarithmic wall function (Eq 2) following the Clauser chart method [1]. Using this method, the streamwise velocity (\bar{U}/U_τ) is plotted in figure 5 with wall scaling for varying values of x/L . The PIV and pitot results agree well with the flow also conforming with a traditional turbulent boundary layer. The PIV profiles of the boundary layer are captured down to a minimum of $z^+ = 30 - 40$, enabling the wake and logarithmic layer to be well resolved. There is a small mismatch in the outer-flow and may be attributed to model vibrations and the error in determining the wall position. The Clauser method is particularly sensitive to the wall position as U_τ is indirectly determined from a fit to the logarithmic region and therefore forces collapse of data in the near wall. Figure 5 (bottom) shows the tail section boundary layer, which departs from a flat plate wall boundary layer profile due to the presence of an adverse pressure gradient. Refer to [7] who measured the static pressure along the same model and also make predictions of the separation lines when the model is inclined.

The first two points from the wall were excluded from the fit to the law of the wall due to the inherent bias error known to exist with PIV very near wall measurements. This bias error is due to the spatial averaging over the PIV interrogation windows in regions of high velocity gradient. To address the spatial averaging limitation of PIV, particle tracking can be used which enables higher accuracy and spatial resolution as well as nearer wall measurements. Vibrations of the model were observed to be of the order 0.05-0.1 mm. The vibrations will mostly affect the inner wall points resulting in smeared mean flow and higher turbulence values. Pre-processing of the images with edge-detection methods can be used to determine the wall position of each image and with such vibration corrections the inner wall measurements should be more accurate.

Turbulence Boundary Layer Profiles

As the hotwire probe measures the response to both the streamwise and vertical velocity component the non-dimensional root mean square velocity magnitude of the PIV data ($U_{XZ\ RMS}/U_\tau$) was used to compare with the hotwire and is shown in figure 6. The magnitudes and profile shapes are very similar, although there is some deviation in the inner layer region and a small offset in the wake region is evident between the PIV and hotwire results.

Boundary Layer Thickness

The boundary layer thickness was determined from a non-linear least squares error fit of the Coles [2] law of the wall and law

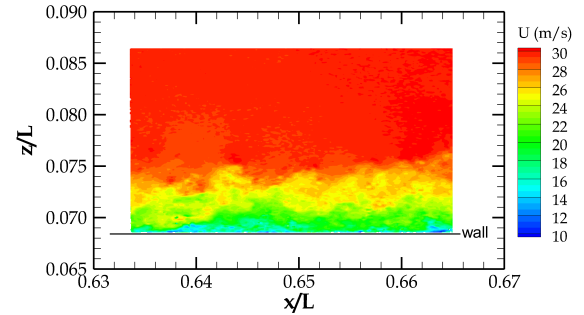


Figure 4: Instantaneous PIV near wall measurements at $0.65L$. Colour coded by the streamwise velocity (U).

of the wake to the PIV mean velocity profile and is plotted in figure 7 along with the flat plate turbulent boundary layer solution. The boundary layer is well resolved by the PIV measurements with over 140 vectors for a 20 mm thick layer. Along the parallel mid-body section the boundary layer thickness is well approximated by the flat plate solution, in the tail section the boundary layer rapidly grows and departs from the flat plate solution due to the presence of an adverse pressure gradient [7].

Longitudinal Distribution of Skin Friction

Comparison of the skin friction coefficient, C_f , determined from Preston tube measurements and law of the wall curve fits to the PIV mean flow data are shown in figure 8. The different methods are reasonably consistent though there is a slight offset between the different techniques. The difference may be due to model vibrations which affect the PIV measurements, whereas the Preston tube is less affected since it is attached to the model.

Conclusions

This study reports long-distance high magnification PIV turbulent boundary layer measurements along a slender body and shows results that compared very well with pitot and hotwire probes. Measurements along the parallel mid-body section of the model were also found to be consistent with the flat plate turbulent boundary layer solution. Spatial averaging within the PIV interrogation windows and vibrations of the model affected the first few wall measurements. Rapid growth of the boundary layer was observed in the tail section and was attributed to the adverse pressure gradient. The skin friction coefficient derived from the PIV measurements agreed well with the Preston tube measurement.

Acknowledgements

The authors acknowledge the support and funding of DST's Maritime Division as well as the support of the Research Training Centre of Naval Design and Manufacturing (ARC IC140100003). Thank you also to Christopher Jones and David Cannistraro from QinetiQ for the development of the lens aperture mount and control software.

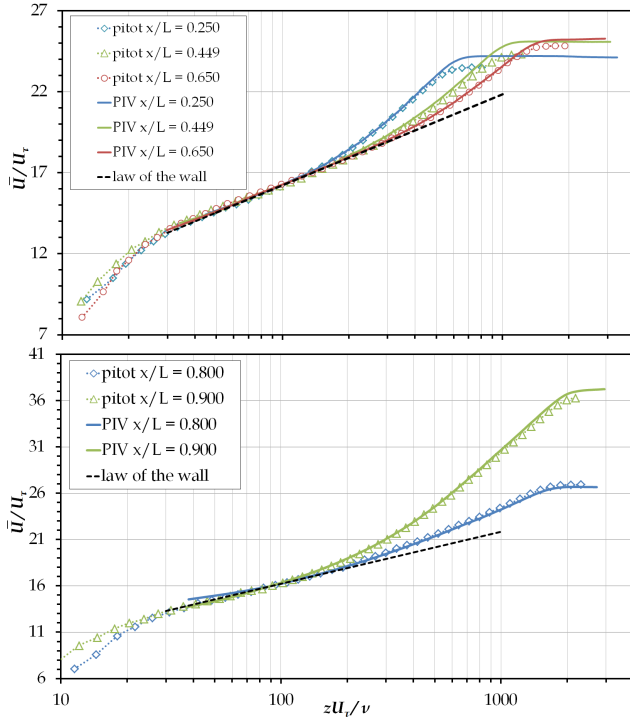


Figure 5: Boundary layer profiles from PIV and pitot measurements compared to law of the wall. Parallel mid-body section of model (top). Tail section of the model (bottom).

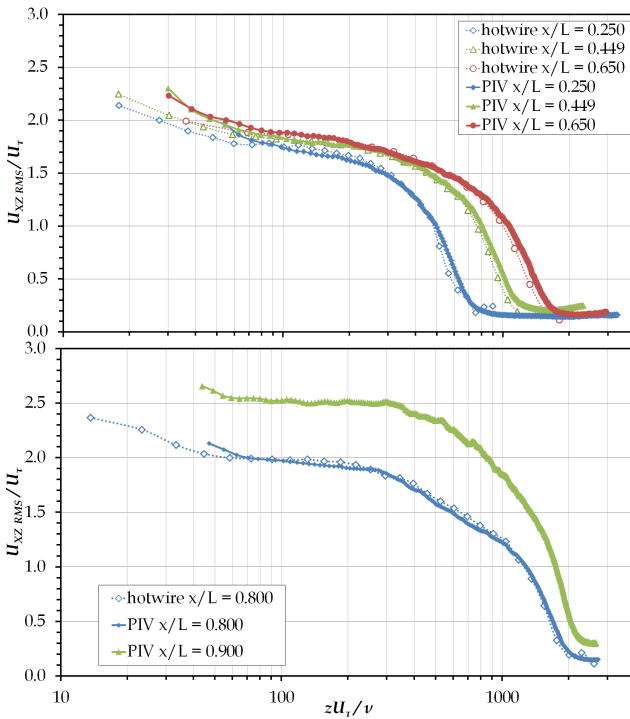


Figure 6: Non-dimensional turbulence ($U_{XZ\ RMS}/U_\tau$) boundary layer profiles from PIV and hotwire measurements with wall scaling. Parallel mid-body section of model (top). Tail section of the model (bottom).

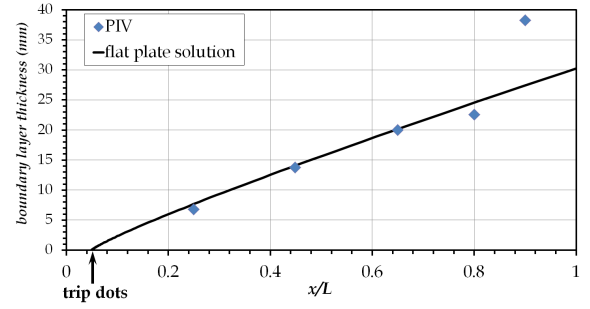


Figure 7: Boundary layer thickness along model length as derived from PIV along with the flat plate solution [2].

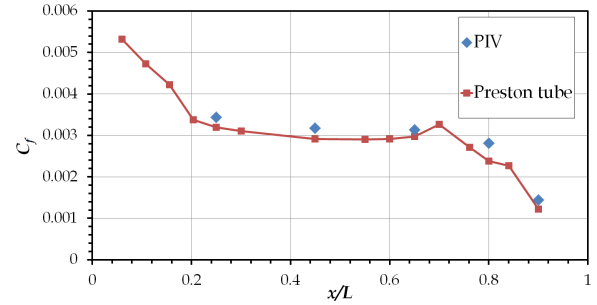


Figure 8: Distribution of streamwise skin friction coefficient C_f along model length inferred from Preston tube and PIV measurements from a curve fit to law of the wall function.

References

- [1] Clauser, F., Turbulent boundary layers in adverse pressure gradients, *J. Aero. Sci.*, **21**, 1954, 91–108.
- [2] Coles, D. E., The law of the wake in the turbulent boundary layer, *J. of Fluid Mechanics*.
- [3] de Silva, C. M., Gnanamanickam, E. P., Atkinson, C., Buchmann, N. A., Hutchins, N., Soria, J. and Marusic, I., High spatial range velocity measurements in a high reynolds number turbulent boundary layer, *Physics of Fluids*, **26**, 2014, 025117.
- [4] Erm, L. P., Calibration of the flow in the extended test section of the low-speed wind tunnel at DSTO, Technical report, DSTO-TR-1073, 2003.
- [5] Henbest, S. M. and Jones, M. B., Transition on a generic submarine model, Technical report, In prep. DST, 2018.
- [6] Jones, M. B., Erm, L. P., Valiyf, A. and Henbest, S. M., Skin-friction measurements on a model submarine, Technical report, DSTO-TR-2898, 2014.
- [7] Lee, S.-K. and Jones, M. B., Surface pressure of inclined slender-body flows, in *21st AFMC*, 2018.
- [8] Patel, V. C., Calibration of the preston tube and limitations on its use in pressure gradients, *J. of Fluid Mechanics*.
- [9] Watmuff, J. H., A high-performance constant-temperature hot-wire anemometer, Technical report, NASA, 1994.